PHYSICAL REVIEW B **107**, 235142 (2023)

Optical signatures of the $J_{\mathrm{eff}} = \frac{1}{2}$ state in Ir^{4+} halides

F. Meggle,[1] M. Mikuta,[1] M. Saule,[1] V. Hermann,[1] N. Khan,[2] A. A. Tsirlin,[2,3] and C. A. Kuntscher[1]

[1] *Experimental Physics II, Institute of Physics, University of Augsburg, 86159 Augsburg, Germany*
[2] *Experimental Physics VI, Center for Electronic Correlations and Magnetism, University of Augsburg, 86159 Augsburg, Germany*
[3] *Felix Bloch Institute for Solid-State Physics, Leipzig University, 04103 Leipzig, Germany*

(Received 31 August 2022; revised 26 April 2023; accepted 6 June 2023; published 23 June 2023)

We study the vibrational and electronic excitations in cubic iridium halides $(\mathrm{NH}_4)_2\mathrm{IrCl}_6$, $\mathrm{K}_2\mathrm{IrCl}_6$, and $\mathrm{K}_2\mathrm{IrBr}_6$ by infrared reflectivity and transmission measurements of single crystals. All three compounds show optical excitations in the energy range of 0.5–0.8 eV, which can be ascribed to $j_{\mathrm{eff}} = \frac{3}{2}$ to $j_{\mathrm{eff}} = \frac{1}{2}$ transitions (spin-orbit excitons), and t_{2g}-to-e_g excitations above $\sim$1 eV. We observe at least two peaks due to spin-orbit excitons in the bromide and four peaks in both chlorides, suggesting local deviations from the cubic symmetry already at room temperature. We further show that the e_g states lie at lower energies in the bromide compared to the chlorides, in agreement with density-functional band-structure calculations.

DOI: 10.1103/PhysRevB.107.235142

I. INTRODUCTION

Iridium oxides containing Ir^{4+} ions with a $5d^5$ electronic configuration have been studied intensively in the past years as relativistic Mott insulators hosting highly anisotropic exchange interactions that may lead, among others, to the Kitaev spin liquid ground state [1–4]. The energy-level scheme of iridates is illustrated in Fig. 1. The octahedral crystal field Δ_{cubic} splits Ir $5d$ states into the t_{2g} and e_g manifolds. The t_{2g} states are further separated into $j_{\mathrm{eff}} = \frac{1}{2}$ and $j_{\mathrm{eff}} = \frac{3}{2}$ states due to the strong spin-orbit (SO) coupling [5]. The rather narrow $j_{\mathrm{eff}} = \frac{1}{2}$ band could, furthermore, be split into lower and upper Hubbard bands due to the on-site Coulomb repulsion, hence, leading to a Mott insulating state. Additionally, distortions of the IrO_6 octahedra can cause a noncubic crystal field that leads to a splitting of the $j_{\mathrm{eff}} = \frac{3}{2}$ states and to a departure from the pure $j_{\mathrm{eff}} = \frac{1}{2}$ state for the local magnetic moments.

Among the prominent examples of this physics, the honeycomb iridates $\mathrm{Na}_2\mathrm{IrO}_3$ and α-$\mathrm{Li}_2\mathrm{IrO}_3$ have raised special attention and extensive research investigations since their Ir^{4+} magnetic moments are close to $j_{\mathrm{eff}} = 1/2$ as witnessed by optical spectroscopy and resonant inelastic x-ray scattering (RIXS) [6–8]. However, magnetic interactions clearly deviate from the pure Kitaev model. Consequently, antiferromagnetic order is observed at low temperatures at ambient pressure. Moreover, the honeycomb iridates undergo a dimerization of the crystal structure under high pressure [9,10].

In this context, the iridium halides $A_2\mathrm{Ir}X_6$ with an antifluorite crystal structure (see Fig. 2), where A can be an alkali metal or NH_4 and X are halogen atoms, have caused attention because of their face-centered cubic symmetry that imparts cubic symmetry also to the isolated $\mathrm{Ir}X_6$ octahedra and may lead to the ideal $j_{\mathrm{eff}} = \frac{1}{2}$ state of Ir^{4+} [11–16]. Indeed, RIXS studies on several $A_2\mathrm{Ir}X_6$ compounds found evidence for a proximity to the $j_{\mathrm{eff}} = \frac{1}{2}$ state, albeit with a small splitting of the excited $j_{\mathrm{eff}} = \frac{3}{2}$ quartet into two doublets due to residual structural distortions driven by soft phonon modes in the crystal structure [13,14]. In this paper, we investigate the electronic ground state of the $A_2\mathrm{Ir}X_6$ materials further by infrared spectroscopy measurements, which enables the study of vibrational and electronic excitations with a better energy resolution as compared to RIXS. The obtained optical conductivity and absorbance spectra are compared to the theoretical density of states for $\mathrm{K}_2\mathrm{IrCl}_6$ and $\mathrm{K}_2\mathrm{IrBr}_6$ as obtained by density-functional-theory (DFT) calculations.

II. METHODS

Single crystals of $\mathrm{K}_2\mathrm{IrCl}_6$, $(\mathrm{NH}_4)_2\mathrm{IrCl}_6$, and $\mathrm{K}_2\mathrm{IrBr}_6$ were grown from water solutions as reported elsewhere [14,17]. The crystal quality was checked by magnetization measurements and by x-ray powder diffraction performed on finely ground crystals selected from the same batch.

The room-temperature infrared spectroscopy measurements were carried out in the frequency range from 120 to 20000 cm^{-1} (15 meV to 2.5 eV) with a Bruker Vertex 80v FTIR spectrometer coupled to a Bruker Hyperion IR-microscope. The reflection measurements were performed on as-grown samples and for the transmission measurements the samples were polished to a thickness between 37 and 25 µm. In the case of $\mathrm{K}_2\mathrm{IrBr}_6$, a crystal was fixed on beeswax for polishing to a smaller thickness of $\sim$20 µm and for mechanical support during the transmission measurements. A commercial unprotected aluminum mirror served as reference for the reflectivity measurements. The real part of the optical conductivity $\sigma_1(\nu)$ was obtained by Kramers-Kronig analysis. To this end, the reflectivity spectra were extrapolated to low energies by using the Lorentz model. The extrapolation above 2.5 eV was calculated by x-ray atomic scattering functions [18]. The absorbance spectra $A(\nu)$ were calculated from the transmission spectra $T(\nu)$ according to $A(\nu) = -\log T(\nu)$. For the transmission measurements the empty beam path served as reference. For all measurements the spectral energy resolution $\Delta\nu$ amounts to $\sim$2 cm^{-1} ($\approx$0.25 meV).

2469-9950/2023/107(23)/235142(6)

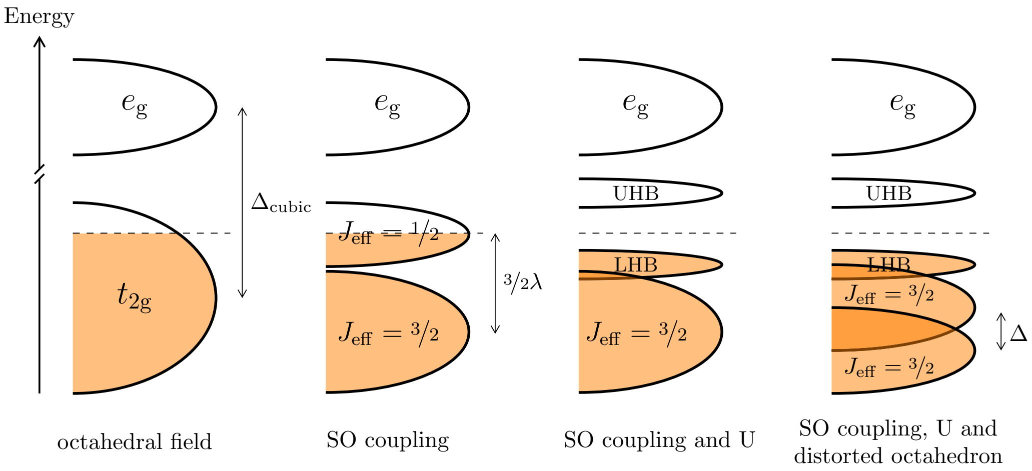

FIG. 1. Energy level scheme of the $5d^5$ orbitals in Ir^{4+}, taking into account the cubic crystal field Δ_{cubic}, spin-orbit coupling (SO) with strength λ, on-site Coulomb repulsion U, and noncubic crystal field Δ. Please note the interrupted energy scale because $\Delta_{\mathrm{cubic}} \gg \lambda$, and that the splittings $3/2\lambda$, U, and Δ are not in scale.

Relativistic DFT band-structure calculations were performed using the FPLO [19] and WIEN2K [20,21] codes with the Perdew-Burke-Ernzerhof exchange-correlation potential [22]. Correlation effects in the Ir $5d$ shell were taken into account on the mean-field DFT+U+SO level. The parameters of the correlated orbital were set to $U_d = 2.2$ eV (K_2IrCl_6) and $U_d = 1.8$ eV (K_2IrBr_6) for the on-site Coulomb repulsion as well as $J_d = 0.3$ eV for Hund's coupling in both compounds. These optimized parameters were previously shown to reproduce magnetic properties of the Ir^{4+} hexahalides [12,14]. Optical conductivity was calculated with the internal routines of WIEN2K [23] on the dense 24×24×24 mesh.

III. RESULTS AND DISCUSSION

The absorbance A and optical conductivity σ_1 spectra of $(NH_4)_2IrCl_6$, K_2IrCl_6, and K_2IrBr_6 are depicted in Figs. 3(a) and 3(b) over a broad frequency range. The optical data reveal the insulating character of all studied compounds. The profiles of the spectra are characterized by peaks centered at 0.6–0.7 eV due to the excitations of electrons from the $j_{\mathrm{eff}} = \frac{3}{2}$ to the $j_{\mathrm{eff}} = \frac{1}{2}$ states (see level scheme in Fig. 1), denoted as spin-orbit excitons in the literature [24], followed by the transitions from the t_{2g} to e_g states at higher energies. The t_{2g}-to-e_g transitions have a large spectral weight, which causes a steep absorption edge at 1.07 eV for K_2IrBr_6 and at 1.64 eV for $(NH_4)_2IrCl_6$ and K_2IrCl_6, with a saturation of the absorbance above 1.2 and 1.7 eV, respectively [see Fig. 3(a)]. Below ~0.5 eV the stretching and bending modes of the IrX_6 octahedra can be observed. They are located at frequencies of 191 and 325 cm^{-1} for $(NH_4)_2IrCl_6$, at 182 and 331 cm^{-1} for K_2IrCl_6, and at 124 and 233 cm^{-1} for K_2IrBr_6. The lower phonon mode frequencies for K_2IrBr_6 as compared to the other two compounds can be qualitatively explained by a simple harmonic-oscillator model with eigenfrequencies $\omega_j = \sqrt{\frac{k_j}{m_j}}$, where m_j is the reduced mass of the ions involved in the vibration, and k_j is the force constant of the mode [25,26]. In the case of $(NH_4)_2IrCl_6$ we observe an additional mode at 130 cm^{-1}, which we assign to NH_4 modes, following the interpretation for K_2IrCl_6 in Ref. [16]. The corresponding modes of the K atoms in K_2IrCl_6 and K_2IrBr_6 are below 120 cm^{-1} [16] and, hence, out of our measurement range. Besides, we observe NH_4^+ molecular vibrations in $(NH_4)_2IrCl_6$ and in the case of K_2IrBr_6 the absorbance spectrum contains additional vibrations that are reminiscent of the OH groups and may indicate partial hydrolysis of the hexahalide ions during crystal growth [see Figs. 3(c) and 3(d)] [27]. We believe that $[IrBr_6]^{2-}$ is more prone to the hydrolisis than $[IrCl_6]^{2-}$, hence, these OH lines are observed in the bromide only. The NH_4^+ and OH^--excitations are better seen in Fig. 5, which will be discussed in more detail later.

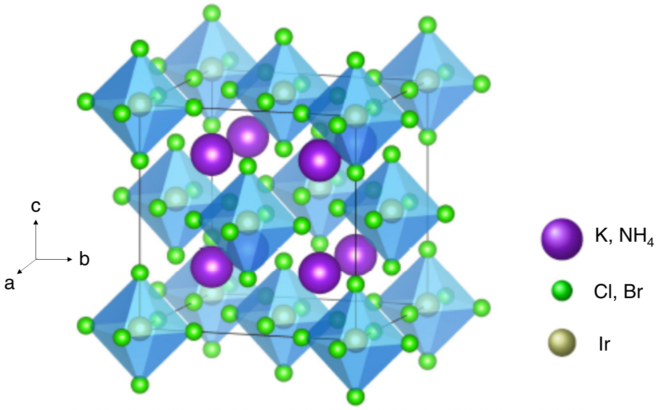

FIG. 2. Crystal structure of iridium halides A_2IrX_6, consisting of isolated IrX_6 octahedra.

Since all materials are opaque above the energy of the absorption edge, the transition energies of the t_{2g}-to-e_g excitations cannot be extracted from the absorbance spectra. Instead, they can be obtained from the high-energy optical conductivity spectra where several well-defined peaks are observed. In order to determine the t_{2g}-to-e_g transition energies, the σ_1 spectra were fitted with the Lorentz model (see Fig. 4), and the so-obtained energies of the most pronounced and well-separated peaks are given in Table I.

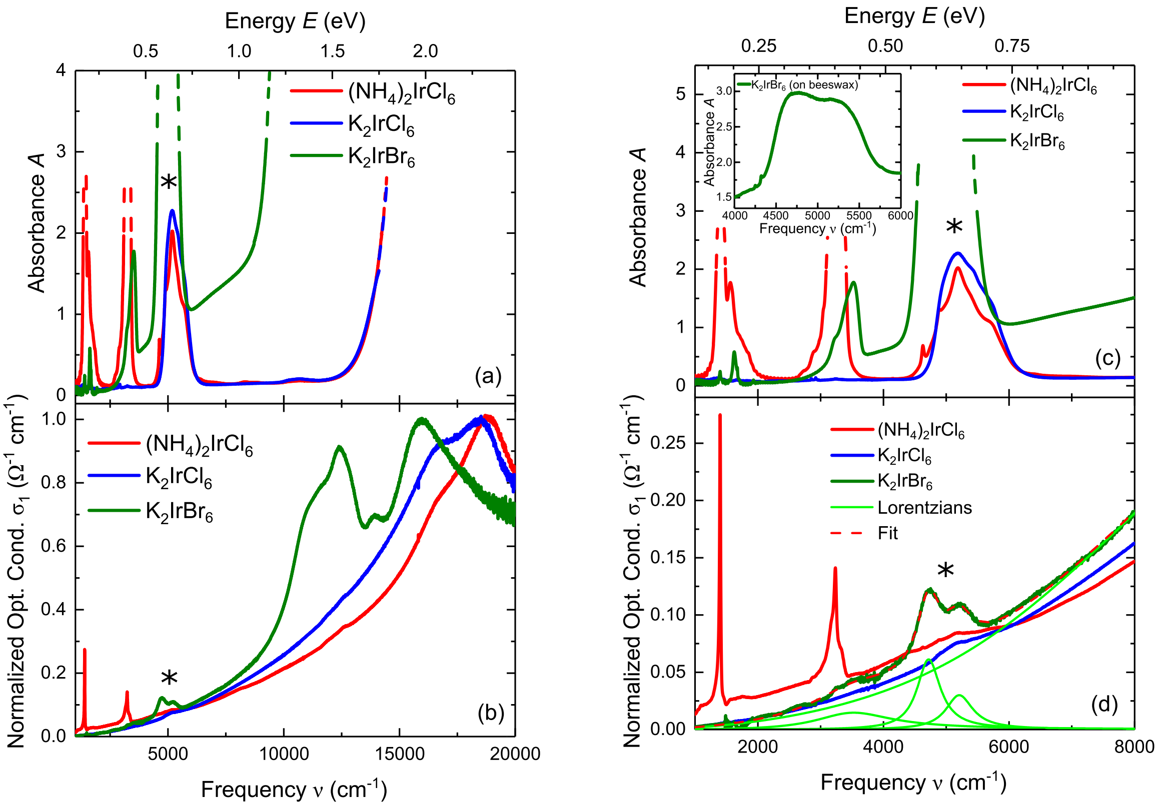

FIG. 3. Absorbance A and optical conductivity σ_1 spectra of three iridium halides: (a) absorbance spectra A in the energy range from 1000 to 20 000 cm^{-1} (0.12 to 2.48 eV) and (b) corresponding optical conductivity σ_1, normalized to the maximum value for comparison reasons, respectively. (c) and (d) are zoom-ins of (a) and (b) on the frequency range from 1000 to 8000 cm^{-1} (0.12 to 0.99 eV). The asterisks mark the excitations from the $j_{\mathrm{eff}} = \frac{3}{2}$ to the $j_{\mathrm{eff}} = \frac{1}{2}$ energy levels. The inset in (c) shows the nonsaturated absorbance spectrum A of a 25-μm thick K_2IrBr_6 sample for frequencies around the $j_{\mathrm{eff}} = \frac{3}{2}$-to-$j_{\mathrm{eff}} = \frac{1}{2}$ excitations.

For K_2IrBr_6 the $j_{\mathrm{eff}} = \frac{3}{2}$-to-$j_{\mathrm{eff}} = \frac{1}{2}$ transitions in the energy range of 0.6–0.7 eV have a larger spectral weight as compared to the other two studied compounds as can be seen in the optical conductivity spectra [Figs. 3(b) and 3(d)] where these transitions are marked with an asterisk. Since the reflectivity measurements on all samples were carried out on as-grown crystal surfaces, the features in the corresponding optical conductivity are broadened by the scattering effect. From the σ_1 spectrum of K_2IrBr_6 we could resolve two $j_{\mathrm{eff}} = \frac{3}{2}$-to-$j_{\mathrm{eff}} = \frac{1}{2}$ transitions. The corresponding absorbance spectra obtained by transmission measurements are less sensitive regarding scattering effects and, therefore, allow a more detailed view on the $j_{\mathrm{eff}} = \frac{3}{2}$-to-$j_{\mathrm{eff}} = \frac{1}{2}$ excitations. However, the high spectral weight of these excitations in K_2IrBr_6 causes a saturation of the absorbance spectrum in this frequency range [Fig. 3(c)]. Even in a very thin crystal with thickness ∼25 μm stabilized by beeswax the absorbance is close to saturation [inset of Fig. 3(c)], and, therefore, it was impossible to resolve all the contributions to the $j_{\mathrm{eff}} = \frac{3}{2}$-to-$j_{\mathrm{eff}} = \frac{1}{2}$ transitions. In contrast, for $(NH_4)_2IrCl_6$ and K_2IrCl_6 all contributions can be well resolved in the absorbance spectra since there is no saturation.

TABLE I. Energies of the t_{2g}-e_g transitions as obtained from the Lorentz fittings of the optical conductivity σ_1 spectra [Fig. 4]. All parameters are in eV. The contribution for $(NH_4)_2IrCl_6$ marked with an asterisk leads to a bump in the spectrum with very small spectral weight.

Material	$\hbar\omega_1$	$\hbar\omega_2$	$\hbar\omega_3$	$\hbar\omega_4$	$\hbar\omega_5$
$(NH_4)_2IrCl_6$	1.55*	2.09	2.32		
K_2IrCl_6	1.59	2.07	2.32		
K_2IrBr_6	1.38	1.55	1.73	1.97	2.21

In the following, we focus on the transitions from the $j_{\mathrm{eff}} = \frac{3}{2}$ to the $j_{\mathrm{eff}} = \frac{1}{2}$ energy levels in the energy range of 0.6–0.7 eV as observed in the experimental optical spectra. For a quantitative characterization, we carried out Lorentz fittings of the absorbance spectra [see Figs. 5(a), 5(b) and 5(d)] and the σ_1 spectrum of K_2IrBr_6 [see Fig. 3(d)]. In the case of K_2IrCl_6, we can resolve four contributions according to the fitting of the absorbance spectrum. For $(NH_4)_2IrCl_6$, the absorbance spectrum shows additional excitations of stretching modes of $(NH_4)^+$ and combinations thereof located at energies of 0.15–0.25 eV and 0.30–0.45 eV [28–30]. We ascribe the sharp peak located at 0.57 eV to a combined vibration of $(NH_4)^+$.

As already mentioned above, for K_2IrBr_6 it is difficult to reveal all contributions to the $j_{\mathrm{eff}} = \frac{3}{2}$-to-$j_{\mathrm{eff}} = \frac{1}{2}$ transitions from the absorbance spectra since the absorbance saturates in the range of 0.6–0.7 eV, even for a very thin crystal stabilized by beeswax [see Figs. 5(c) and 5(d)]. The additional excitations in the spectrum at around 0.35 eV are due to beeswax [31], and the spectra of the bromide compound contain hints

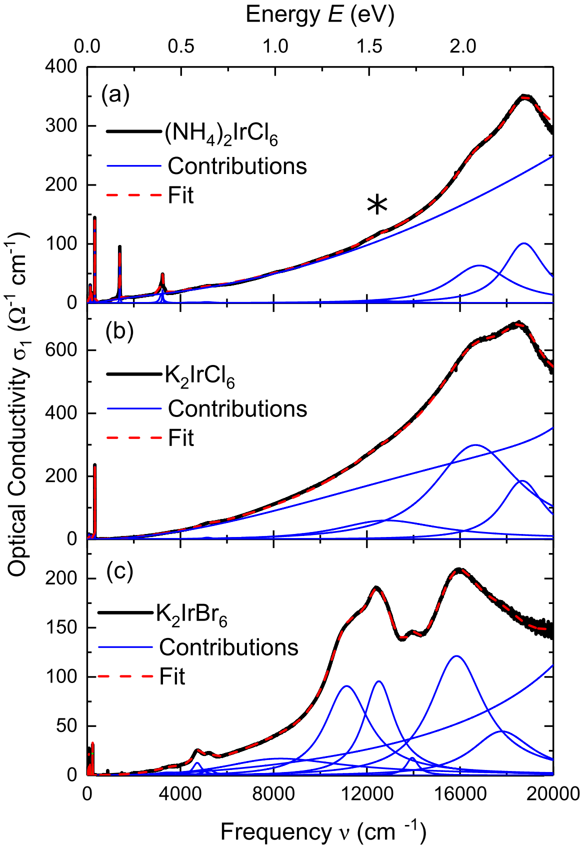

FIG. 4. Fits of the optical conductivity spectra σ_1 of three iridium halides with the Lorentz model together with the Lorentz contributions. The asterisk in panel (a) indicates the small bump, which is also marked with an asterisk in Table I.

for OH excitations. Based on the fit of the σ_1 spectrum [see Fig. 3(d)] we could identify only two contributions to the $j_{\mathrm{eff}} = \frac{3}{2}$-to-$j_{\mathrm{eff}} = \frac{1}{2}$ excitations in K_2IrBr_6 since a broad background obscures features with less spectral weight. Hence, for K_2IrBr_6 we could determine the energies of two $j_{\mathrm{eff}} = \frac{3}{2}$ to $j_{\mathrm{eff}} = \frac{1}{2}$ transitions but cannot rule out additional transitions.

The energies of the $j_{\mathrm{eff}} = \frac{3}{2}$-to-$j_{\mathrm{eff}} = \frac{1}{2}$ transitions in all studied compounds are listed in Table II. According to Ref. [32] these transition energies can be used to estimate the value of the spin-orbit coupling constant λ since their average energy corresponds to $\frac{3}{2}\lambda$. For all studied iridium halide compounds, the values of λ lie in the range of 410–439 meV (see Table II), which is in good agreement with the values reported in Refs. [13,14] obtained by RIXS studies with an overall energy resolution of ~35 meV. However, in contrast to the RIXS results, we could resolve four contributions for the compounds $(NH_4)_2IrCl_6$ and K_2IrCl_6 due to the very good energy resolution of infrared spectroscopy (~0.25 meV), and this most probably holds also for K_2IrBr_6.

TABLE II. Energies of the transitions from the $j_{\mathrm{eff}} = \frac{3}{2}$ to the $j_{\mathrm{eff}} = \frac{1}{2}$ energy levels as obtained from the Lorentz fittings of the absorbance spectra [Figs. 5(a), 5(b) and 5(d)] and the σ_1 spectrum [Fig. 3(d)], together with the spin-orbit coupling strength λ (see text). All parameters are in meV.

Material	$\hbar\omega_1$	$\hbar\omega_2$	$\hbar\omega_3$	$\hbar\omega_4$	λ
$(NH_4)_2IrCl_6$	605	643	671	708	438
K_2IrCl_6	616	641	674	710	440
K_2IrBr_6 (absorbance)	582	654			412
K_2IrBr_6 (σ_1)	585	646			410

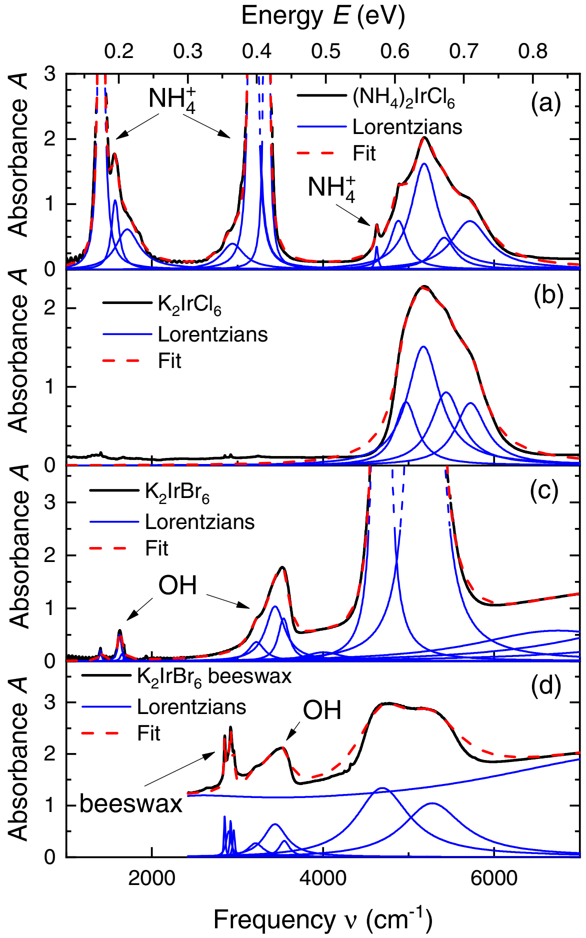

FIG. 5. Absorbance spectrum A with the corresponding Lorentz fit and Lorentz contributions for (a) $(NH_4)_2IrCl_6$, (b) K_2IrCl_6, (c) K_2IrBr_6, and (d) a thinner K_2IrBr_6 crystal fixed on beeswax. The vibrational excitations related to NH_4^+, OH^-, and beeswax are indicated.

It has been argued that the observation of two excitations of the intra-t_{2g} levels in the RIXS spectra can be attributed to a splitting of the $j_{\mathrm{eff}} = \frac{3}{2}$ quartet state into two doublet states due to noncubic crystal field [13]. However, such a splitting cannot explain the four excitation peaks in the infrared spectra. For an explanation of this finding, we carried out orbital-resolved DFT band-structure calculations, and the calculated density of states for K_2IrCl_6 and K_2IrBr_6 are shown in Fig. 6. Accordingly, the lower Hubbard band of $j_{\mathrm{eff}} = \frac{1}{2}$ is strongly mixed with $j_{\mathrm{eff}} = \frac{3}{2}$ and, moreover, with the ligand p states that are dominant even in the vicinity of the Fermi level (the inset of Fig. 6). Possible explanations for our findings of

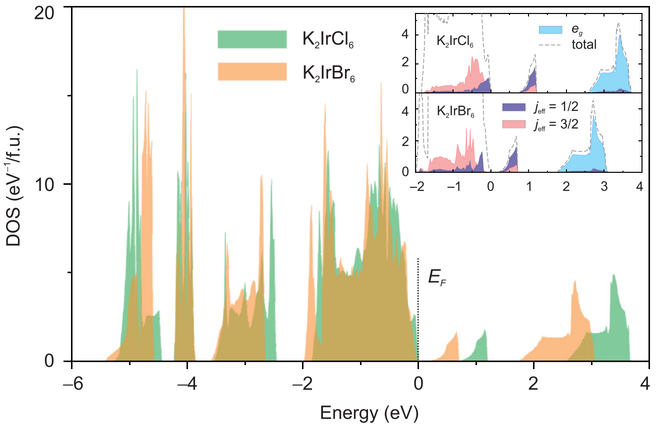

FIG. 6. Comparison of DFT+U+SO density of states (DOS) for cubic K$_2$IrCl$_6$ and K$_2$IrBr$_6$. The Fermi level is at zero energy. In the case of bromide, the lower value of U_d and the smaller crystal-field splitting both shift Ir e_g states to lower energies. The inset: Orbital-resolved DOS for K$_2$IrCl$_6$ and K$_2$IrBr$_6$.

four intra-t_{2g} transitions are, therefore, (i) a finite width of both $j_{\rm eff} = \frac{1}{2}$ and $j_{\rm eff} = \frac{3}{2}$ bands, which cause multiple absorption features since optical spectroscopy probes the transitions at all points in the Brillouin zone and (ii) transitions between the lower and the upper Hubbard bands of $j_{\rm eff} = \frac{1}{2}$, which coincide with the $j_{\rm eff} = \frac{3}{2}$-to-$j_{\rm eff} = \frac{1}{2}$ transitions. Besides, the structural distortion in K$_2$IrCl$_6$ and (NH$_4$)$_2$IrCl$_6$, whose nature is presently unknown, might lead to the formation of several Ir^{4+} sites. It is important to note that recent Raman spectroscopy studies on K$_2$IrCl$_6$ single crystals also observed multiple $j_{\rm eff} = \frac{3}{2}$-to-$j_{\rm eff} = \frac{1}{2}$ transitions from which $\lambda \approx 0.41$ eV was extracted, in good agreement with our results [16]. The multiple excitations were attributed to spin-orbit excitons with a possible coupling to electron-hole excitations of the $j_{\rm eff} = \frac{1}{2}$ orbitals.

Consistent with the above interpretation, the calculated optical conductivity σ_1 spectra of K$_2$IrBr$_6$ and K$_2$IrCl$_6$, depicted in Fig. 7, contain several excitation peaks in the energy range 0.4–0.7 eV. These $j_{\rm eff} = \frac{3}{2}$ to $j_{\rm eff} = \frac{1}{2}$ and $j_{\rm eff} = \frac{1}{2}$ to $j_{\rm eff} = \frac{1}{2}$ transitions appear with a rather large spectral weight in the theoretical spectra, which might be a downside of the mean-field treatment of electronic correlations within DFT+U+SO. The steep onset of the optical conductivity at around 2.8 and 3.6 eV is ascribed to t_{2g}-to-e_g transitions for K$_2$IrBr$_6$ and K$_2$IrCl$_6$, respectively. The different energetic positions of the onset can be traced back to the calculated DOS where the Ir e_g states are shifted to lower energies in the case of the bromide compound (see Fig. 6). This happens because of the smaller cubic crystal-field splitting in the bromide since the Ir-ligand distances are longer compared to the chlorides.

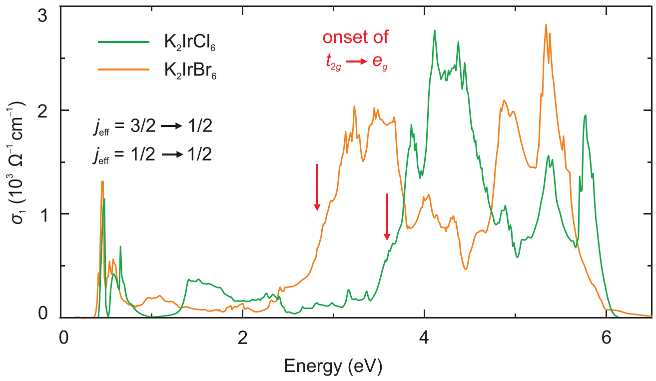

FIG. 7. Comparison of the optical conductivity σ_1 calculated for K$_2$IrBr$_6$ and K$_2$IrCl$_6$ on the DFT+U+SO level.

Additionally, the lower value of the Hubbard parameter U_d may lead to the smaller splitting between the filled t_{2g} states and empty e_g states in the bromide. This finding is in qualitative agreement with the experimental data [see Fig. 3(b)]; however, theory overestimates the energy of the t_{2g}-to-e_g transitions as compared to the experimental results.

IV. CONCLUSION

The absorbance and optical conductivity spectra of the nominally cubic iridium halides (NH$_4$)$_2$IrCl$_6$, K$_2$IrCl$_6$, and K$_2$IrBr$_6$ show vibrational modes of the IrX_6 octahedra and NH$_4^+$ molecular vibrations below ~0.5 eV and electronic transitions between $j_{\rm eff} = \frac{3}{2}$ and $j_{\rm eff} = \frac{1}{2}$ states and between the lower and the upper Hubbard bands of $j_{\rm eff} = \frac{1}{2}$ at energies 0.6–0.7 eV, followed by t_{2g}-to-e_g transitions above ~1 eV. We confirm that the splitting of the SO exciton peaks occurs already at room temperature. This indicates local deviations from the cubic symmetry and the departure from the ideal $j_{\rm eff} = \frac{1}{2}$ state of Ir^{4+} even if macroscopic symmetry probed by x-ray diffraction remains cubic. Additionally, in contrast to the recent RIXS measurements, we could resolve four contributions to the $j_{\rm eff} = \frac{3}{2}$-to-$j_{\rm eff} = \frac{1}{2}$ excitations for (NH$_4$)$_2$IrCl$_6$ and K$_2$IrCl$_6$ due to the advanced energy resolution of infrared spectroscopy. The lower energies of the electronic excitations in the experimental optical spectra of K$_2$IrBr$_6$ are due to the lower on-site Coulomb repulsion U_d and the smaller crystal-field splitting according to our DFT band structure calculations. The optical data of K$_2$IrBr$_6$ and K$_2$IrCl$_6$ are in qualitative agreement with the calculated optical conductivity spectra.

ACKNOWLEDGMENT

Computations for this work were performed (in part) using resources of the Leipzig University Computing Center.

---

[1] A. Kitaev, Anyons in an exactly solved model and beyond, Ann. Phys. **321**, 2 (2006).

[2] W. Witczak-Krempa, G. Chen, Y. B. Kim, and L. Balents, Correlated quantum phenomena in the strong spin-orbit regime, Annu. Rev. Condens. Matter Phys. **5**, 57 (2014).

[3] J. G. Rau, E. K.-H. Lee, and H.-Y. Kee, Spin-orbit physics giving rise to novel phases in correlated systems: Iridates and related materials, Annu. Rev. Condens. Matter Phys. **7**, 195 (2016).

[4] S. M. Winter, A. A. Tsirlin, M. Daghofer, J. van den Brink, Y. Singh, P. Gegenwart, and R. Valentí, Models and materials for

generalized Kitaev magnetism, J. Phys.: Condens. Matter **29**, 493002 (2017).

[5] B. J. Kim, Hosub Jin, S. J. Moon, J.-Y. Kim, B.-G. Park, C. S. Leem, Jaejun Yu, T. W. Noh, C. Kim, S.-J. Oh, J.-H. Park, V. Durairaj, G. Cao, and E. Rotenberg, Novel $J_{\rm eff} = 1/2$ Mott State Induced by Relativistic Spin-Orbit Coupling in Sr_2IrO_4, Phys. Rev. Lett. **101**, 076402 (2008).

[6] V. Hermann, J. Ebad-Allah, F. Freund, I. M. Pietsch, A. Jesche, A. A. Tsirlin, J. Deisenhofer, M. Hanfland, P. Gegenwart, and C. A. Kuntscher, High-pressure versus isoelectronic doping effect on the honeycomb iridate Na_2IrO_3, Phys. Rev. B **96**, 195137 (2017).

[7] V. Hermann, J. Ebad-Allah, F. Freund, A. Jesche, A. A. Tsirlin, P. Gegenwart, and C. A. Kuntscher, Optical signature of the pressure-induced dimerization in the honeycomb iridate $\alpha-$ Li_2IrO_3, Phys. Rev. B **99**, 235116 (2019).

[8] H. Gretarsson, J. P. Clancy, X. Liu, J. P. Hill, E. Bozin, Y. Singh, S. Manni, P. Gegenwart, J. Kim, A. H. Said, D. Casa, T. Gog, M. H. Upton, H.-S. Kim, J. Yu, V. M. Katukuri, L. Hozoi, J. van den Brink, and Y.-J. Kim, Crystal-Field Splitting and Correlation Effect on the Electronic Structure of A_2IrO_3, Phys. Rev. Lett. **110**, 076402 (2013).

[9] V. Hermann, M. Altmeyer, J. Ebad-Allah, F. Freund, A. Jesche, A. A. Tsirlin, M. Hanfland, P. Gegenwart, I. I. Mazin, D. I. Khomskii, R. Valentí, and C. A. Kuntscher, Competition between spin-orbit coupling, magnetism, and dimerization in the honeycomb iridates: $\alpha-Li_2IrO_3$ under pressure, Phys. Rev. B **97**, 020104(R) (2018).

[10] J. P. Clancy, H. Gretarsson, J. A. Sears, Y. Singh, S. Desgreniers, K. Mehlawat, S. Layek, G. Kh. Rozenberg, Y. Ding, M. H. Upton, D. Casa, N. Chen, J. Im, Y. Lee, R. Yadav, L. Hozoi, D. Efremov, J. van den Brink, and Y.-J. Kim, Pressure-driven collapse of the relativistic electronic ground state in a honeycomb iridate, npj Quantum Mater. **3**, 35 (2018).

[11] T. Birol and K. Haule, $J_{\rm eff} = 1/2$ Mott-Insulating State in Rh and Ir Fluorides, Phys. Rev. Lett. **114**, 096403 (2015).

[12] N. Khan, D. Prishchenko, Y. Skourski, V. G. Mazurenko, and A. A. Tsirlin, Cubic symmetry and magnetic frustration on the fcc spin lattice in K_2IrCl_6, Phys. Rev. B **99**, 144425 (2019).

[13] D. Reig-i-Plessis, T. A. Johnson, K. Lu, Q. Chen, J. P. C. Ruff, M. H. Upton, T. J. Williams, S. Calder, H. D. Zhou, J. P. Clancy, A. A. Aczel, and G. J. MacDougall, Structural, electronic, and magnetic properties of the nearly ideal $J_{\rm eff} = \frac{1}{2}$ iridium halides, Phys. Rev. Mater. **4**, 124407 (2020).

[14] N. Khan, D. Prishchenko, M. H. Upton, V. G. Mazurenko, and A. A. Tsirlin, Towards cubic symmetry for Ir^{4+}: Structure and magnetism of the antifluorite K_2IrBr_6, Phys. Rev. B **103**, 125158 (2021).

[15] L. Bhaskaran, A. N. Ponomaryov, J. Wosnitza, N. Khan, A. A. Tsirlin, M. E. Zhitomirsky, and S. A. Zvyagin, Antiferromagnetic resonance in the cubic iridium hexahalides $(NH_4)_2IrCl_6$ and K_2IrCl_6, Phys. Rev. B **104**, 184404 (2021).

[16] S. Lee, B. H. Kim, M.-J. Seong, and K.-Y. Choi, Noncubic local distortions and spin-orbit excitons in K_2IrCl_6, Phys. Rev. B **105**, 184433 (2022).

[17] N. Khan, D. Khalyavin, P. Manuel, and A. A. Tsirlin, Magnetic order in $(NH_4)_2IrCl_6$, (unpublished).

[18] D. B. Tanner, Use of x-ray scattering functions in Kramers-Kronig analysis of reflectance, Phys. Rev. B **91**, 035123 (2015).

[19] K. Koepernik and H. Eschrig, Full-potential nonorthogonal local-orbital minimum-basis band-structure scheme, Phys. Rev. B **59**, 1743 (1999).

[20] P. Blaha, K. Schwarz, G. K. H. Madsen, D. Kvasnicka, J. Luitz, R. Laskowski, F. Tran, and L. D. Marks, WIEN2k, An Augmented Plane Wave + Local Orbitals Program for Calculating Crystal Properties (Karlheinz Schwarz, Techn. Universität Wien, Austria, 2018).

[21] P. Blaha, K. Schwarz, F. Tran, R. Laskowski, G. K. H. Madsen, and L. D. Marks, WIEN2k: An APW+lo program for calculating the properties of solids, J. Chem. Phys. **152**, 074101 (2020).

[22] J. P. Perdew, K. Burke, and M. Ernzerhof, Generalized Gradient Approximation Made Simple, Phys. Rev. Lett. **77**, 3865 (1996).

[23] C. Ambrosch-Draxl and J. O. Sofo, Linear optical properties of solids within the full-potential linearized augmented planewave method, Comput. Phys. Commun. **175**, 1 (2006).

[24] Jungho Kim, D. Casa, M. H. Upton, T. Gog, Young-June Kim, J. F. Mitchell, M. van Veenendaal, M. Daghofer, J. van den Brink, G. Khaliullin, and B. J. Kim, Magnetic Excitation Spectra of Sr_2IrO_4 Probed by Resonant Inelastic X-Ray Scattering: Establishing Links to Cuprate Superconductors, Phys. Rev. Lett. **108**, 177003 (2012).

[25] P. W. Atkins, in *Physical Chemistry* (Oxford University Press, Oxford, 1986), p. 455.

[26] G. Caimi, L. Degiorgi, P. Lemmens, and F. C. Chou, Analysis of the phonon spectrum in the titanium oxyhalide TiOBr, J. Phys.: Condens. Matter **16**, 5583 (2004).

[27] J. Gilchrist, Low temperature dielectric relaxations in ammonium hexachlorostannate and some other antifluorites, J. Phys. Chem. Solids **50**, 857 (1989).

[28] V. Busigny, P. Cartigny, P. Philippot, and M. Javoy, Quantitative analysis of ammonium in biotite using infrared spectroscopy, Am. Mineral. **89**, 1625 (2004).

[29] I. A. Oxton, O. Knop, and M. Falk, Infrared spectra of the ammonium ion in crystals. I. Ammonium hexachloroplatinate(IV) and hexachlorotellurate(IV), Can. J. Chem. **53**, 2675 (1975).

[30] L. F. H. Bovey, The infrared absorption and reflection spectra of the ammonium halides, J. Opt. Soc. Am. **41**, 836 (1951).

[31] L. Svečnjak, G. Baranović, M. Vinceković, S. Prđun, D. Bubalo, and I. T. Gajger, An approach for routine analytical detection of beeswax adulteration using FTIR-ATR spectroscopy, J. Apic. Sci. **59**, 37 (2015).

[32] A. A. Aczel, J. P. Clancy, Q. Chen, H. D. Zhou, D. Reig-i Plessis, G. J. MacDougall, J. P. C. Ruff, M. H. Upton, Z. Islam, T. J. Williams, S. Calder, and J.-Q. Yan, Revisiting the Kitaev material candidacy of Ir^{4+} double perovskite iridates, Phys. Rev. B **99**, 134417 (2019).